Journal of Cerebral Blood Flow & Metabolism (2014) 34, 768–775

www.jcbfm.com

ORIGINAL ARTICLE

Parenchymal spin-lock fMRI signals associated with cortical spreading depression

Joonas A Autio[1,2], Artem Shatillo[1], Rashid Giniatullin[1] and Olli H Gröhn[1]

We found novel types of parenchymal functional magnetic resonance imaging (fMRI) signals in the rat brain during large increases in metabolism. Cortical spreading depression (CSD), a self-propagating wave of cellular activation, is associated with several pathologic conditions such as migraine and stroke. It was used as a paradigm to evoke transient neuronal depolarization leading to enhanced energy consumption. Activation of CSD was investigated using spin-lock (SL), diffusion, blood oxygenation level-dependent and cerebral blood volume fMRI techniques. Our results show that the SL-fMRI signal is generated by endogenous parenchymal mechanisms during CSD propagation, and these mechanisms are not associated with hemodynamic changes or cellular swelling. Protein phantoms suggest that pH change alone does not explain the observed SL-fMRI signal changes. However, increased amounts of inorganic phosphates released from high-energy phosphates combined with pH changes may produce SL- power-dependent longitudinal relaxation in the rotating frame ($R_{1\rho}$) changes in protein phantoms that are similar to those observed during CSD, as seen before in acute ischemia under our experimental conditions. This links SL-fMRI changes intimately to energy metabolism and supports the use of the SL technique as a new, promising functional approach for noninvasive imaging of metabolic transitions in the active or pathologic brain.

Journal of Cerebral Blood Flow & Metabolism (2014) **34,** 768–775; doi:10.1038/jcbfm.2014.16; published online 5 February 2014

Keywords: adenosine; BOLD contrast; MRI; pH; spreading depression

INTRODUCTION

Functional magnetic resonance imaging (fMRI) is an invaluable noninvasive imaging technique for the study of brain activity in health and disease. The blood oxygen level-dependent (BOLD) fMRI signal consists of both hemodynamic and metabolic contributions and thus provides an indirect indicator of neural activity.[1] However, the relationship between BOLD signals and neuronal activity is known to be very complex, particularly under pathologic conditions.[2,3] There is also a persistent lack of validation of the extent BOLD fMRI that is determined by parenchymal metabolic activity and changes in hemodynamic components, which are expected to extend fMRI localization to supporting arterioles and draining veins. Therefore, there is a strong need for novel functional imaging modalities that enable more specific measurements of neurometabolic activity with good spatial and temporal resolution.

Recently, there has been considerable interest in developing alternative MRI methods to achieve neuronal or metabolic measures *via* water signals.[4,5] One of these methods is spin-lock (SL) fMRI, which utilizes longitudinal rotating frame relaxation ($R_{1\rho} = 1/T_{1\rho}$). This method is a powerful tool to probe different dynamic processes that influence the image contrast by adjusting the SL power ($B_{1,SL}$).[6] Several *in vitro* studies have established that the SL technique is sensitive to chemical exchange processes between water and hydroxyl, amine and amide groups, solute properties (pH and phosphates) and dipolar fluctuations, which constitute a large part of the parenchymal *in vivo* imaging contrast.[7–10] These properties are closely associated with tissue homeostasis and energy status. In principle, a perturbation in homeostatic equilibrium and energy state may translate into changes in endogenous parenchymal signals detectable using SL-fMRI and provide indirect measures of *in vivo* metabolic status *via* water signals. Indeed, a recent study showed a decrease in $R_{1\rho}$ during human visual system stimulation at 3 T.[11] It was proposed that localized, activity-evoked acidosis may be detectable using SL-fMRI. This view on the role of pH activity was further supported by localized ^{1}H and ^{31}P spectroscopic findings. However, in human studies it is difficult to exclude the contribution of direct cerebral blood volume (CBV) fluctuations to SL-fMRI and an earlier study has proposed that signal changes may be ascribed to changes in partial volume effects.[12] A recent carefully designed study separated CBV, cerebrospinal fluid, and parenchymal signals, and found a small parenchymal $R_{1\rho}$ response in the middle cortical layer during cat visual cortex stimulation at 9.4 T.[13] However, in this case it was argued that their finding of functional $R_{1\rho}$ *decrease* cannot be explained by acidosis because mild hypercapnia conversely induced $R_{1\rho}$ *increase* at a $B_{1,SL}$ of 500 Hz. Tentatively, the study suggested that a functional $R_{1\rho}$ decrease is possibly caused by a transient decrease in glucose concentration. Clearly, the origins of the promising SL-fMRI contrast require further investigations, importantly with the exclusion of hemodynamic factors.

The aim of the present study was to investigate brain parenchymal SL-fMRI signals evoked by strong activation in rats. To address this possibility, cortical spreading depression (CSD) was used as a stimulation paradigm in combination with an SL-fMRI technique. Cortical spreading depression, a self-propagating wave of neuronal depolarization, occurs with several neurologic

[1]Department of Neurobiology, A. I. Virtanen Institute, University of Eastern Finland, Kuopio, Finland and [2]Medical Research Center Oulu, Oulu University Hospital and University of Oulu, Oulu, Finland. Correspondence: JA Autio, Department of Neurobiology, A. I. Virtanen Institute, University of Eastern Finland, Neulaniementie 2, Kuopio 70700, Finland.
E-mail: joonas.autio@ppshp.fi
This work was supported by the Academy of Finland, UEF-Brain—University of Eastern Finland strategic funding, and Biocenter Finland mobility funding.
Received 3 September 2013; revised 30 December 2013; accepted 8 January 2014; published online 5 February 2014

disorders such as migraine aura, stroke, and epilepsy.[14] It is associated with large but transient disturbances in ion homeostasis, neuronal swelling, subsequent decrease in adenosine triphosphate (ATP) and phosphocreatine (PCr) levels and acidosis.[15–18] Here we use BOLD, CBV, diffusion, and SL techniques, which have different sensitivities to hemodynamic, neuronal, and metabolic changes, to better understand neurometabolic events during CSD. In addition, protein samples were studied to investigate the effects of phosphate containing compounds and pH upon SL MRI contrast.

MATERIALS AND METHODS

Animal Preparation

All animal procedures were approved by the Committee for the Welfare of Laboratory Animals of the University of Eastern Finland and the Provincial Government of Kuopio, Finland, and conducted in accordance with the guidelines set by the European Community Council Directives 86/609/EEC. Male Sprague-Dawley rats, 10 to 12 weeks old (340 ± 40 g, $n = 14$), were initially anesthetized with isoflurane carried in a mixture of O_2 (30%) and N_2 (70%) for surgical preparation. A 3-mm^2 cranial window was made in the parietal bone above the visual cortex (5 mm posterior to the bregma and 2.5 mm lateral to the midline) and meninges was carefully removed to expose the cortical surface. A polyethylene micro tube (PE10, BD, Becton, Dickinson and Company, Franklin Lakes, NJ, USA) was glued (Permabond 2011 cyanacrylate, Permabond LLC, Pottstown, PA, USA) to the skull adjacent to the exposed cortex for potassium chloride delivery. The cranial window was covered with saline-moisturized filter paper to prevent exposed regions from dehydration. A catheter was inserted into the femoral artery for blood sampling. In CBV-weighted (CBV-w) experiments, an intravenous catheter was inserted for injections of an intravascular contrast agent (8 mg/kg, ultra-small superparamagnetic iron oxide (USPIO); Sinerem, Guerbet, France). After surgery, the anesthesia was switched to urethane (intraperitoneally, 1.25 g/kg). Body temperature was maintained at 37°C using a water heating pad and the respiratory rate was monitored using a pressure-transducing probe (SA Instruments, Stony Brook, NY, USA) during all experiments. Cortical spreading depression was evoked with the application of 10 μL of 1 mol/L potassium chloride.

Magnetic Resonance Imaging Acquisition

All MRI experiments were performed on a 9.4-T/31-cm horizontal magnet system interfaced to a DirectDrive console (Agilent Inc., Palo Alto, CA, USA). A half-volume quadrature coil (Virtumed LLC, Minneapolis, MN, USA) was used to achieve high sensitivity and to obtain high $B_{1,SL}$ values. T_1-weighted gradient-echo scout images were acquired to identify the anatomic structures of the brain. A 2-mm coronal plane with 25×25 mm field-of-view perpendicular to the surface of the cortex was selected 3.1 mm ventrally to the level of the bregma and all subsequent experiments were performed on that slice. Fast spin-echo anatomic reference images were acquired with a 128×128 matrix, 48 ms effective echo time (TE), 8 train length, and 16 ms echo spacing. All subsequent experiments were performed with single-shot spin-echo echo-planar imaging using a 64×64 matrix size.

B_1 maps were quantified by incrementing the length of a square pulse before echo-planar imaging to calibrate transmission power. The SL preparation consisted of two 4 ms adiabatic half-passage pulses bridged by an on-resonance SL period, and this was followed with crusher gradients.[19] $R_{1\rho}$ was measured using six SL times (TSL) ranging between 10 and 80 ms, with a $B_{1,SL}$ of 500 and 6,000 Hz. Repetition time of 3 seconds and TE of 22 ms were used. For subsequent fMRI runs, the interleaved data acquisition scheme consisted of three images: control image without SL preparation and two images with a 50-ms TSL using the $B_{1,SL}$ of 500 and 6,000 Hz. The repetition time of the imaging scheme was 6 seconds. Each fMRI trial lasted 45 minutes.

To minimize the effect of coupling between applied and internal gradients, bipolar diffusion sensitizing gradients were used.[20–22] Diffusion weighting was applied only before a 180° refocusing pulse on all three axes simultaneously. Apparent diffusion coefficient (ADC) was measured using seven b values ranging between 0 and 1.2 ms/μm^2 with 5.1 ms diffusion time (Δ), 5.0 ms diffusion gradient duration (δ), and 30 ms TE. Diffusion-weighted (DW)-fMRI trials were acquired with three b values: 0, 0.6, and 1.2 ms/μm^2. The repetition time of the imaging scheme was 6 seconds.

Protein and Metabolite Experiments

Heat-denatured 10% bovine albumin serum samples with varying concentrations of inorganic phosphates, adenosine tri-, di-, and monophosphate (ATP, ADP, and AMP), PCr, creatine (Cr) and with varying pH were prepared in 0.1 mol/L Tris-buffered saline solution. Metabolite phantoms with varying concentrations of PCr, Cr, and glucose were prepared in 0.1 mmol/L phosphate-buffered saline solution and titrated to pH of 7.4. Imaging was performed with a 19-mm quadrature volume coil (Rapid Biomedical, Rimpar, Germany). $R_{1\rho}$ was measured with eight $B_{1,SL}$ values ranging between 500 and 6,000 Hz and with eight TSLs ranging between 10 and 100 ms. Images were collected with the fast spin-echo technique.

Data Analyses

Functional MRI images were normalized with preCSD levels. The relative fMRI images were subtracted from the relative SL-weighted or DW images at each time point. The difference images were used to generate SL or ADC activation maps. The mean signal intensities in the fMRI signals were calculated within a region of interest after regional time courses were shifted to have the same onset time. To determine peak signal changes, mean signal time course was smoothed with a 3-point temporal window to reduce noise. Relative CBV changes were determined with BOLD and baseline signal correction.[23] To compare temporal characteristics, signal time courses were smoothed with a 3-point temporal window and normalized to the peak signal change. The threshold for onset time and duration was defined as 10% of the peak change.

Throughout the manuscript the following terminology is used: experiments performed *without* SL weighting are defined as BOLD fMRI, and in the presence of USPIO are defined as CBV-w fMRI. Experiments performed *with* SL weighting are defined as SL-w fMRI, and the presence of USPIO is indicated in parentheses SL-w(USPIO). Results obtained by subtracting the BOLD fMRI from SL-w fMRI are defined as SL-fMRI, and in the presence of USPIO results obtained by subtracting the CBV-w fMRI from SL-w(USPIO) fMRI are defined as SL(USPIO)-fMRI. $B_{1,SL}$ utilized is indicated in the subscript, i.e., SL_{6000Hz} and $SL(USPIO)_{6000Hz}$. It is important to keep in mind that in the CBV-w fMRI and SL-w(USPIO) fMRI experiments the intravascular signal is attenuated by an intravascular contrast agent. In contrast, in the BOLD fMRI and SL-w fMRI experiments the intravascular signal may influence on the results.

RESULTS

Spin Lock-Functional Magnetic Resonance Imaging Reveals Prominent Changes in Endogenous Contrast During Cortical Spreading Depression

A local application of K^+ onto the visual cortex initiated CSD and large spatiotemporal fMRI changes were observed (Figure 1A; Supplementary Video S1). As the CSD propagated through the ipsilateral cortex, the initial positive response was followed by a negative BOLD fMRI signal, which did not return to baseline during the 45-minute scan. The SL-w increased CSD-associated fMRI signal changes as indicated by SL-fMRI activation maps (Figures 1B and 1C; Supplementary Videos S2 and S3), obtained by subtracting BOLD images from SL-w images. Spin lock activation maps showed spatiotemporal differences when compared with BOLD activation maps (Figures 1A to 1C; Supplementary Videos S1 to S3). SL_{500Hz} and SL_{6000Hz} fMRI responses preceded BOLD fMRI responses. The SL_{6000Hz} response exhibited increases in the whole ipsilateral cortex and showed a larger spatial extent at the cortical area when compared with positive BOLD. An inspection of postCSD BOLD undershoot indicates that the whole ipsilateral cortex was influenced by CSD. Similar findings were observed in all animals and trials ($n = 5$, 14 trials).

To obtain a quantitative estimation of the signal changes, we next averaged the relative signal time courses based on anatomically selected regions of interest. Within the region of interest (Figure 1D, inset), the SL_{500Hz} and SL_{6000Hz} $R_{1\rho}$ values were 19.8 ± 0.4 and 11.7 ± 0.4 1/s, respectively. The relative time courses of BOLD fMRI indicated that the initial BOLD overshoot was followed by a prolonged negative BOLD signal (Figure 1D). Both SL-w_{500Hz} and SL-w_{6000Hz} signals showed prominent changes when compared with the BOLD fMRI signal (Figure 1D). The peak

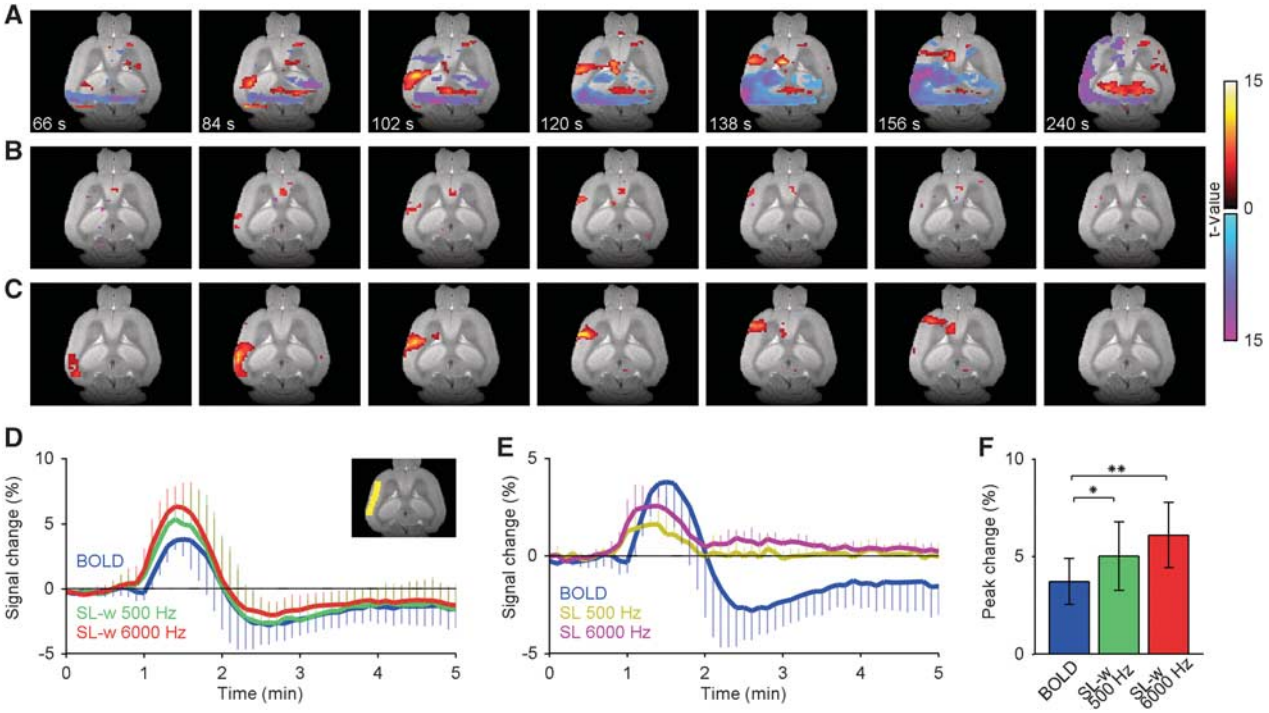

Figure 1. Cortical spreading depression (CSD) evokes substantial changes in blood oxygen level-dependent (BOLD) functional magnetic resonance imaging (fMRI) and spin-lock (SL) signals in the rat brain cortex. (**A**) Typical activation patterns during propagation of CSD as characterized by BOLD fMRI. The SL activation maps have a power ($B_{1,SL}$) of (**B**) 500 Hz and (**C**) 6,000 Hz. Signal increases (warm colors) and decreases (cold colors) indicate *t* values. The maps are superimposed on the high-resolution anatomic reference image. (**D**) Relative BOLD fMRI (blue), SL-w_{500Hz} (green), and SL-w_{6000Hz} (red) time courses averaged across five subjects (mean ± s.d.). The inset image shows a typical region of interest (yellow). (**E**) Relative SL_{500Hz} (dark yellow) and SL_{6000Hz} (dark red) responses compared with BOLD fMRI response (blue). (**F**) Peak signal change averaged across five subjects (± s.d., $^*P<0.05$, $^{**}P<0.001$, paired *t*-test).

signal changes of 5.0 ± 1.8% ($P<0.05$) and 6.1 ± 1.7% ($P<0.001$) for SL-w_{500Hz} and SL-w_{6000Hz}, respectively, were substantially larger than the 3.7 ± 1.2% BOLD response (Figure 1F). To visualize the signal change contributing to the SL period without BOLD contribution, the differences between BOLD and SL-w signals are plotted in Figure 1E. In agreement with the activation maps, relative SL time courses exhibited earlier and abrupt increases in magnitude when compared with BOLD. Peak $\Delta R_{1\rho}$ was − 0.32 ± 0.05 and − 0.51 ± 0.19 1/s for B_1 500 and 6,000 Hz, respectively. The SL_{6000Hz} response was followed by a prolonged but transient overshoot, which outlasted the BOLD overshoot.

Exclusion of Hemodynamic Factors

Because blood presumably influenced SL-fMRI results we next administered paramagnetic USPIO particles to the vasculature with an aim to remove the intravascular signal. As the CSD was initiated, spatiotemporally propagating decreases in the CBV-w fMRI signal were observed (Figure 2A; Supplementary Video S4). This indicates that relaxation caused by increased paramagnetic contrast agent content due to vasodilatation surpasses the positive BOLD effect (Figure 2D). In contrast to SL_{500Hz} fMRI results, the SL_{500Hz}(USPIO) fMRI signal was negligible (Figures 2B, 2D, and 2F, $n=5$, 12 trials). This result indicates that the aforementioned SL_{500Hz} response originated from partial volume effects (Figures 1B and 1E). The relative SL_{6000Hz}(USPIO) time course exhibited substantial increases in signal intensity (Figures 2C and 2E; Supplementary Video S5). The peak signal change was significantly different between CBV-w measures (− 3.1 ± 1.6%) and that with SL-w_{6000Hz}(USPIO) values of − 0.7 ± 1.6% (Figure 2F, $P<0.001$). The SL responses are compared with the CBV-w time course in Figure 2E. Peak $\Delta R_{1\rho}$ was − 0.50 ± 0.09 1/s for SL_{6000Hz} response.

One hypothetical explanation for the SL responses is that they may reflect changes in extravascular magnetic field inhomogeneities, produced by paramagnetic blood deoxyhemoglobin or contrast agent. However, there is both experimental and theoretical evidence that vascular tissue-induced magnetic field variations have a negligible effect at the SL fields used in this study.[13,24,25] To address this possibility, after the blood contribution was attenuated by initial contrast agent application, we administered additional paramagnetic injections (1 mg/kg) into the vasculature ($n=2$, 4 trials). In agreement with previous reports, increases in microscopic field gradients decreased the fMRI signal but had a negligible effect during SL-w (Figure 2G). Paired *t*-tests revealed no significant difference in $R_{1\rho}$ before and after the additional contrast agent injections ($P=0.8$), indicating that the blood contribution was attenuated by the initial bolus administration and that microscopic field inhomogeneities had a negligible effect on SL attenuation. Regardless of the opposite polarity of fMRI signal changes in BOLD and CBV-w experiments, the SL_{6000Hz} and SL_{6000Hz}(USPIO) exhibited increased signal intensities, which also contradicts the notion that microscopic field variations are a signal source. Another hypothetical explanation is that the SL_{6000Hz}(USPIO) response reflects changes in CBV. However, according to the theory, if intravascular and cerebrospinal fluid contributions are negligible, then changes in CBV have no influence on apparent SL relaxation properties. Nevertheless, to confirm this idea we next administered acetazolamide intraperitoneally, which is a clinically used pharmaceutical carbonic anhydrase inhibitor, to test the influence of vasodilatation upon SL responses ($n=2$, 50 mg/kg). Consistent with the theory, SL weighting exhibited no changes in the acetazolamide-evoked CBV-w response (− 3.2 ± 0.3), indicating that changes in CBV had a negligible effect on the SL(USPIO) signal (Figure 2H). Taken together, our results indicate that the

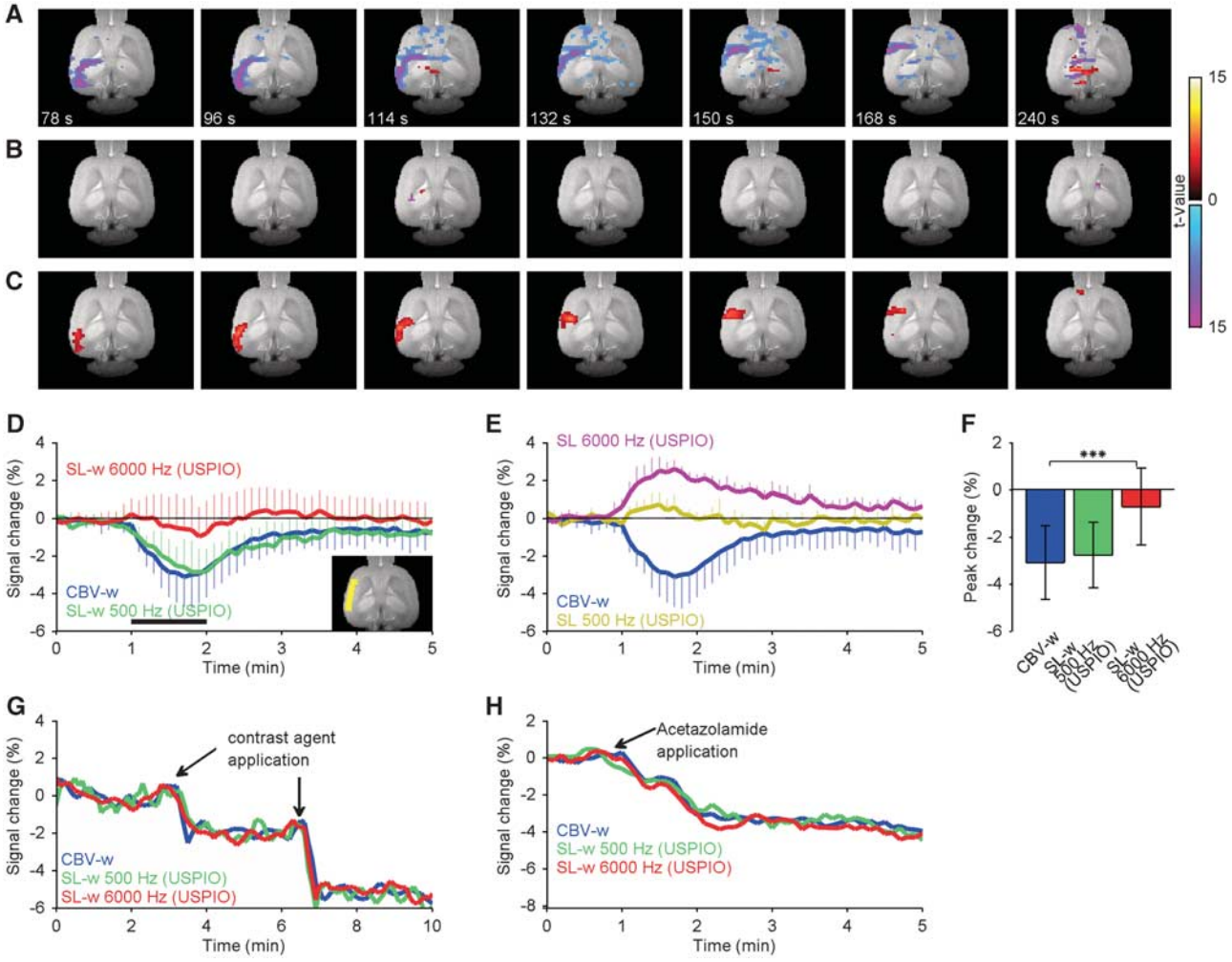

Figure 2. In combination with the cerebral blood volume (CBV)-weighted (w) technique, spin-lock (SL) functional magnetic resonance imaging (fMRI) reveals prominent increases in parenchymal signals during cortical spreading depression (CSD). (**A**) Typical activation maps during propagation of CSD as characterized by CBV-w fMRI. The SL activation patterns have a power ($B_{1,SL}$) of (**B**) 500 Hz and (**C**) 6,000 Hz. Signal increases (warm colors) and decreases (cold colors) indicate *t* values. The maps are superimposed on the high-resolution anatomic reference image. (**D**) Relative CBV-w fMRI (blue), SL-w_{500Hz}(USPIO) (green), and SL-w_{6000Hz}(USPIO) (red) time courses averaged across five subjects (mean ± s.d.). The inset image shows a typical region of interest (yellow). (**E**) Relative SL_{500Hz}(USPIO) (dark yellow) and SL_{6000Hz}(USPIO) (dark red) responses compared with CBV-w fMRI response (blue). (**F**) Peak signal change averaged across five subjects (± s.d., ***$P<0.001$, paired *t*-test). Relative to CBV-w fMRI, SL-w signals were unaltered by (**G**) extravascular field gradients induced by additional contrast agent applications or (**H**) vasodilatation evoked by acetazolamide injection. USPIO, ultra-small superparamagnetic iron oxide.

SL_{6000Hz}(USPIO) fMRI signal is influenced by endogenous mechanisms that are fundamentally different from the BOLD response and originate from the brain parenchyma.

Cellular Swelling

To investigate the possibility that the changes in the SL-fMRI signal are associated with depolarization-induced neuronal swelling, our next approach was to measure the temporal dynamics of tissue water mobility as characterized by ADC.[18,26] Because changes in cerebral blood flow and CBV may influence ADC measurements, we used USPIO particles to attenuate the intravascular signal. As the CSD propagated, decreases in the CBV-w fMRI signal were observed (Figure 3A), consistent with results from the SL-w(USPIO) group. Both $b=0.6$ and $b=1.2$ ms/μm^2 exhibited prominent increases in the CBV-w fMRI signal through the ipsilateral cortex, and only the activation patterns of the latter are shown in Figure 3B (Supplementary Video S6). The activation maps suggest that the diffusion slowdown response precedes CBV increases, and it shows a similar extent when compared with the SL_{6000Hz}(USPIO) response (Figure 2C). Within the region of interest, ADC values were $0.57\pm0.02\,\mu m^2$/ms (Figure 3C, inset). The averaged relative responses with and without DW are shown in Figure 3C ($n=4$, trials 6). The peak signal changes were clearly larger with both $b=0.6$ (2.4 ± 1.1%, $P<0.001$) and $b=1.2$ ms/μm^2 (7.4 ± 1.6%, $P<0.001$) when compared with −2.7 ± 1.2% in the CBV-w fMRI response (Figure 3E). Note that in this set of CBV-w experiments, to accompany motion-probing gradients, the TE was longer and therefore the CBV-w fMRI responses were larger in magnitude when compared with the SL-w(USPIO) group (Figure 2F). The subtracted relative ADC and CBV-w responses are compared in Figure 3D. Peak ΔADC was $-0.084\pm0.008\,\mu m^2$/ms.

Temporal Characteristics

To obtain a quantitative estimation of differences in temporal characteristics between the methods, we analyzed peak normalized

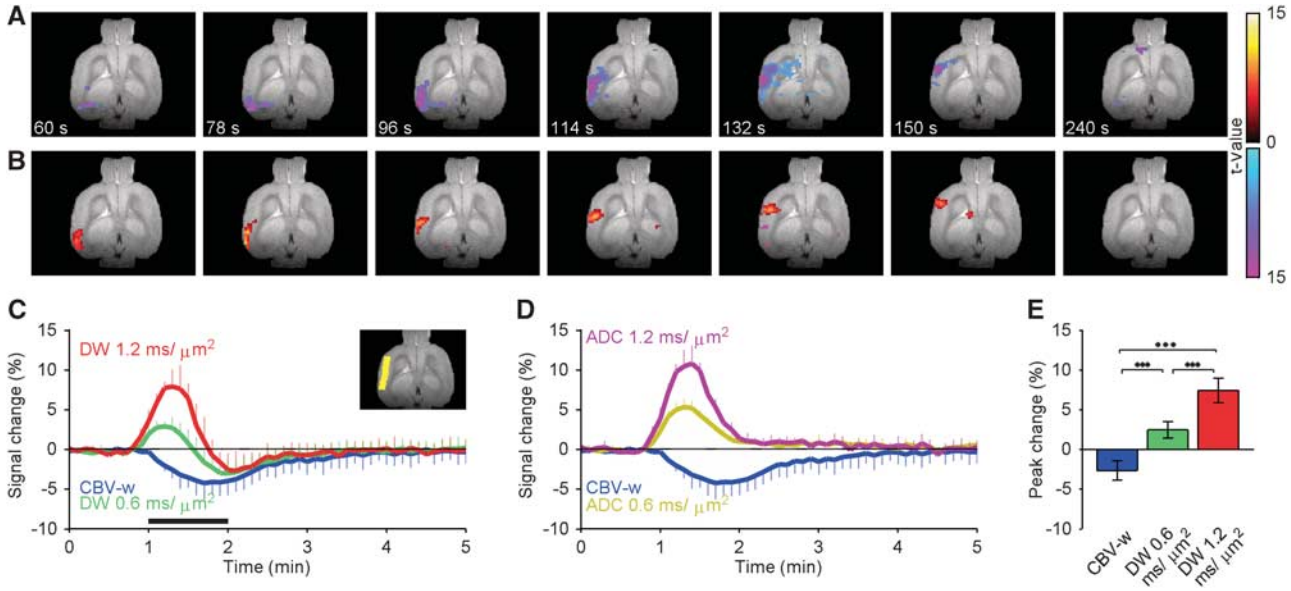

Figure 3. In combination with the cerebral blood volume (CBV)-weighted (w) technique, diffusion-weighted (DW)-fMRI revealed prominent decreases in parenchymal water mobility during cortical spreading depression (CSD). (**A**) Typical activation maps during propagation of CSD as characterized by CBV-w fMRI. (**B**) The apparent diffusion coefficient (ADC) activation patterns with a *b* value of 1.2 ms/μm^2. Signal increases (warm colors) and decreases (cold colors) indicate *t* values. The maps are superimposed on the high-resolution anatomic reference image (**C**). Relative CBV-w fMRI (blue) with *b* values of 0.6 (green) and 1.2 ms/μm^2 (red) DW time courses averaged across four subjects (mean ± s.d.). The inset image shows a typical region of interest (yellow). (**E**) Relative ADC responses with *b* value 0.6 (dark yellow) and 1.2 ms/μm^2 (dark red) compared with a CBV-w fMRI response (blue). (**F**) Peak signal change averaged across four subjects (± s.d., ***$P<0.001$, paired *t*-test). fMRI, functional magnetic resonance imaging.

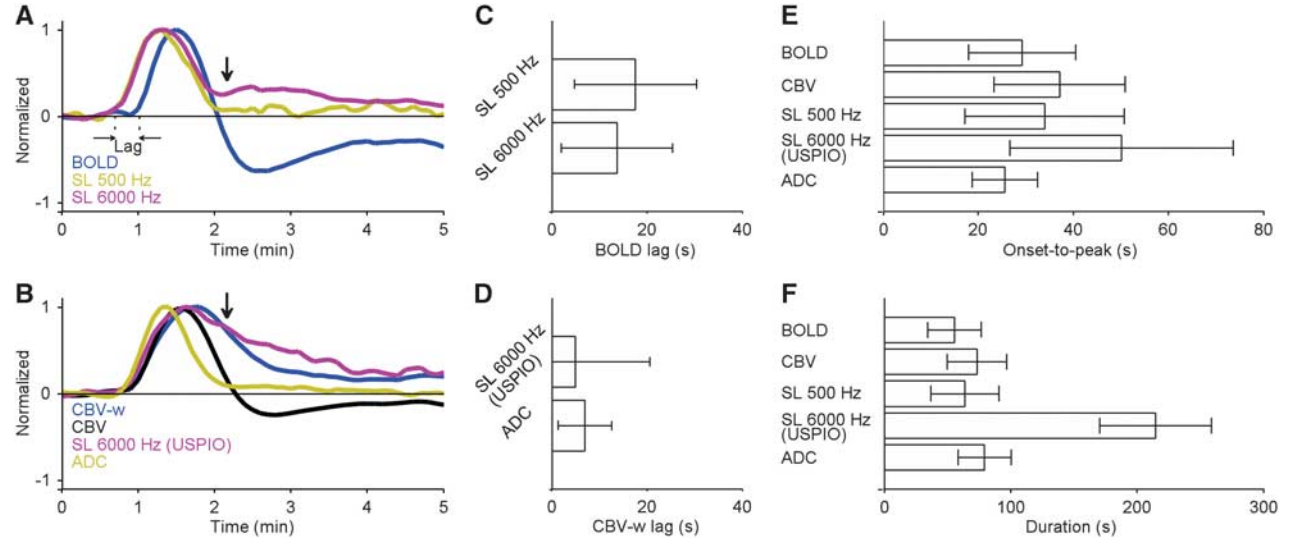

Figure 4. Summary of temporal characteristics. (**A**) Comparison of peak normalized blood oxygen level-dependent (BOLD) (blue) and the corresponding spin-lock (SL) SL_{500Hz} (dark yellow) and SL_{6000Hz} (dark red) time courses. (**B**) Comparison of peak normalized cerebral blood volume (CBV)-weighted (w) (blue), CBV (black), and the corresponding SL_{6000Hz}(USPIO) (dark red) and apparent diffusion coefficient (ADC) (dark yellow) time courses. Note that the direction of the CBV-w response was inverted for comparison. Note the difference between SL_{6000Hz} and SL_{6000Hz}(USPIO) temporal characteristics (vertical black arrows). (**C**) Latency between BOLD and SL_{500Hz} and SL_{6000Hz} onset. (**D**) Latency between the corresponding CBV-w and SL_{6000Hz}(USPIO) and ADC onset. (**E**) Summary histogram of time from onset to the maximum signal change. (**F**) Summary histogram of signal change duration. SL_{6000Hz}(USPIO) was used in (**E**) and (**F**) because it does not have confounding effects of blood signal unlike SL_{6000Hz} response. The time courses were smoothed with a 3-point time vector. Data are presented as mean (± s.d.). USPIO, ultra-small superparamagnetic iron oxide.

signal time courses (Figure 4). Figures 4A and 4C indicate that the onset of normalized SL_{500Hz} and SL_{6000Hz} responses, obtained by subtracting BOLD signal from SL-w signal, preceded the normalized BOLD response by 17 ± 12 ($P<0.001$) and 14 ± 12 seconds ($P<0.001$), respectively. In contrast, the normalized SL_{6000Hz}(USPIO) response, obtained by subtracting CBV-w signal from SL-w(USPIO) signal, showed no systematic differences in onset time with CBV-w signal (Figures 4B and 4D). A normalized CBV time course,

determined from averaged data across TE 22 ms subjects, indicates that vasodilatation was followed by persistent vasoconstriction (Figure 2B). Interestingly, SL_{6000Hz} returned to baseline faster than SL_{6000Hz}(USPIO) response (Figures 4A and 4B, vertical black arrows). This difference may be ascribed to partial volume effect arising from blood signal in the former experiment.

Because the SL_{6000Hz}(USPIO) response does not have confounding partial volume effects, it was used for subsequent analyses. The normalized SL_{6000Hz}(USPIO) exhibited a significantly longer onset-to-peak time of 50 ± 23 seconds (Figure 4E, $P < 0.01$) and positive response of 214 ± 45 seconds (Figure 4F, $P < 0.001$) when compared with BOLD and ADC. Combined, the temporal analyses indicated that the SL_{6000Hz}(USPIO) response was influenced by mechanisms that differ from hemodynamic changes and cellular swelling. Both with $b = 0.6$ and 1.2 ms/μm^2, ADC responses had similar temporal characteristics and the average is shown in Figure 4B. The normalized ADC response preceded the CBV-w response by 7 ± 6 seconds (Figure 4D, $P < 0.01$), in accordance with earlier reports.[26,27]

$R_{1\rho}$ Is Sensitive to Inorganic Phosphate, pH, and Metabolite Concentrations

To investigate plausible signal origins of the SL_{6000Hz}(USPIO) response, we next measured the effects of inorganic phosphates and phosphate containing compounds upon $R_{1\rho}$ in heat-denatured protein samples at 37°C. Figure 5A indicates that $R_{1\rho}$, both at low and at high $B_{1,SL}$, is strongly dependent on the inorganic phosphate concentration. All ATP, ADP, and AMP influenced $R_{1\rho}$ to the same extent (Figure 5B). Together, these results indicated that ATP hydrolyses to ADP and AMP, and these molecules reduce $R_{1\rho}$ *via* the release of inorganic phosphate groups. To investigate how metabolites influence $R_{1\rho}$, PCr, Cr, and glucose, samples were investigated at 37°C. Phosphocreatine exhibited negligible $R_{1\rho}$ changes within the physiologic concentration and the $B_{1,SL}$ range used (Figure 5C). Figures 5D and 5E indicate that Cr and glucose contribute to $R_{1\rho}$ at low $B_{1,SL}$, but at high $B_{1,SL}$ the effects are negligible. These results indicate that consumption of PCr to Cr increases $R_{1\rho}$ at low $B_{1,SL}$ values ($< 1{,}000$ Hz). Figure 5F indicates that a decrease in pH increases $R_{1\rho}$ at low $B_{1,SL}$ values and decreases $R_{1\rho}$ at high $B_{1,SL}$ values, in agreement with previous results for immobilized protein and *in vivo* hypercapnia.[9,13] During CSD, ATP and PCr levels were reduced by 50% and pH decreased by 0.3 units.[15–17] To obtain insight on how energy metabolism may have influenced our SL-fMRI results, phantoms with comparable changes were investigated (Figure 5G). Phantoms suggested that during CSD a $R_{1\rho}$ decrease is observed only at a high $B_{1,SL}$ range ($> 2{,}100$ Hz) with negligible changes at a low $B_{1,SL}$ range. These results are in agreement with our functional observations, thus SL-fMRI may reflect the combined effect of a deficit in ATP, PCr levels and acidification, linking exhaustion of energy reserves to larger $R_{1\rho}$ decreases (Figure 5G).[28]

DISCUSSION

The present study shows the novel finding that CSD evokes changes in the brain parenchymal fMRI contrast detectable with the $R_{1\rho}$ technique. Importantly, the SL_{6000Hz}(USPIO) response could not be ascribed either to hemodynamic mechanisms or to cellular swelling. Temporal characteristics, different from the time profile of the BOLD signal, suggest nonhemodynamic slow metabolic mechanisms as a source. Thus, the $R_{1\rho}$ technique provides a novel approach to measure endogenous fMRI signals associated with enhanced brain metabolism. This approach may have a wide range of applications in biology and medicine.

There could be several parenchymal metabolic mechanisms for the SL_{6000Hz}(USPIO) fMRI response. It is well established that *in vivo* $R_{1\rho}$ is influenced by chemical exchange between water and labile protons and the ratio between exchange rate and chemical shift difference between exchangeable sites ($k/\Delta\omega$), which is dependent on pH and phosphorus compound concentrations (Figure 5). Plausible explanations for functional observations are acidic pH shift,[11,13,24] a decrease in glucose level *via* anaerobic glycolysis,[13] and consumption of high-energy phosphates, ATP and PCr, with a

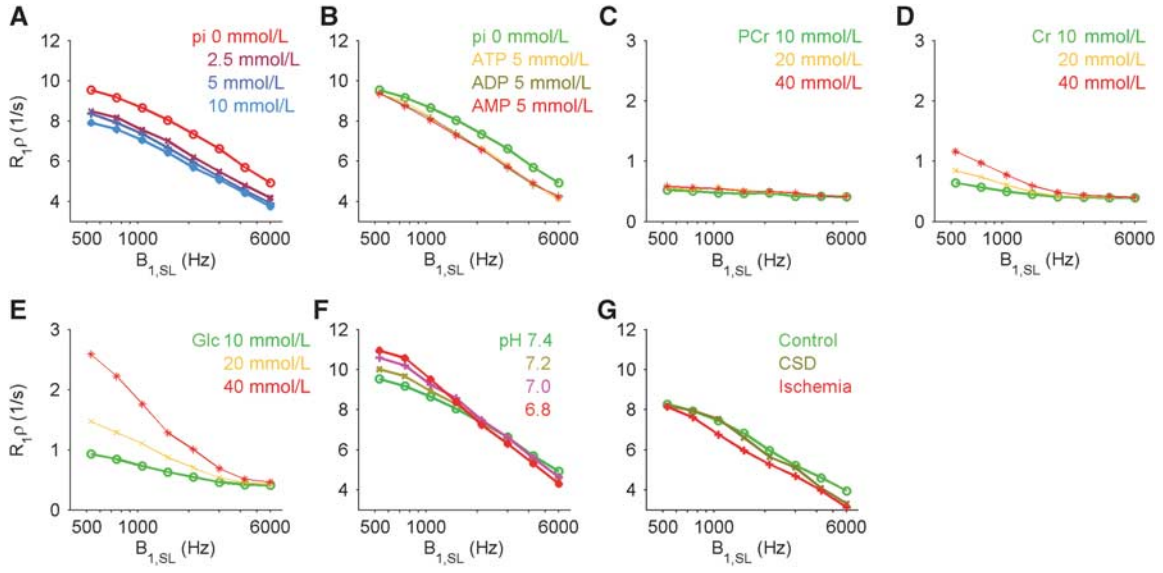

Figure 5. Longitudinal relaxation in the rotating frame ($R_{1\rho}$) as a function of spin-lock (SL) power ($B_{1,SL}$) in bovine albumin serum (BSA) protein phantoms and in metabolites with varying concentrations. BSA protein with pH 7.4, (**A**) inorganic phosphate (pi) and (**B**) adenosine tri-, di-, and monophosphate (ATP, ADP, and AMP) reduced $R_{1\rho}$. (**C**) Phosphocreatine (PCr) exhibit negligible $R_{1\rho}$ changes whereas (**D**) creatine and (**E**) glucose exhibit $R_{1\rho}$ changes only at low $B_{1,SL}$ values. (**F**) BSA protein samples pH dependence increases and decreases $R_{1\rho}$ with low and high $B_{1,SL}$, respectively. (**G**) Plausible cortical spreading depression and ischemia-evoked $R_{1\rho}$ changes induced by decreases in ATP and PCr levels and pH. Control: ATP and PCr 5 mmol/L, pH 7.4, CSD: ATP, ADP, PCr, and creatine (Cr) 2.5 mmol/L, pi 5 mmol/L, pH 7.1 and ischemia: AMP and Cr 5 mmol/L, pi 15 mmol/L and pH 6.8.

release of inorganic phosphate ions. Indeed, acidification and large decreases in glucose, ATP, and PCr concentrations have all been reported during CSD.[15,29] These metabolic events may contribute to SL-fMRI and the source is likely complex. In this study, $B_{1,SL}$ values of 500 and 6,000 Hz were used to probe functional signals since they exhibit different sensitivities to changes in pH, metabolites, and inorganic phosphorus compounds. We found substantial signal increases using only a $B_{1,SL}$ of 6,000 Hz (Figure 2). Thus, the pH alone cannot explain our $\Delta R_{1\rho}$ observations since both our phantom results (Figure 5F) and previous hypercapnia results indicate that acidification increases $R_{1\rho}$ substantially at a $B_{1,SL}$ of 500 Hz.[9,13] While decreases in glucose concentration may decrease $R_{1\rho}$, and in part counter the effects of acidification at $B_{1,SL}$ 500 Hz, the glucose contribution is negligible with the high $B_{1,SL}$ approach (Figure 5E). Furthermore, glucose concentration remained depleted for 30 minutes,[30] which does not match with our $R_{1\rho}$ time course. A decrease in PCr/Cr ratio through creatine kinase reaction may increase $R_{1\rho}$ at low $B_{1,SL}$ values, but this contribution is also negligible with $B_{1,SL}$ 6,000 Hz (Figures 5C and 5D). The difference between PCr and Cr $R_{1\rho}$ may be ascribed to $k/\Delta\omega$ ratios of 0.03 and 0.2, respectively.[31] Elevated inorganic phosphate alone is also unable to explain our functional observation since our phantom results indicate that the release of inorganic phosphates decreases $R_{1\rho}$ at $B_{1,SL}$ 500 (Figure 5A). Our observations can mainly be attributed to the combined effects of acidification and increase in inorganic phosphate concentration (Figure 5G). These observations may also explain our previous findings in stroke, which suggests that pH is not the predominant contributor to the regulation of $R_{1\rho}$.[32,33]

Inorganic phosphates may have a crucial role in $R_{1\rho}$ because phosphates catalyze several fold alternations in proton exchange rates between water molecules and protons of nonequivalent chemical environments.[7] However, the effect of catalysis to exchange rate is difficult to predict since the relationship between catalyst concentration and exchange is nonlinear. Furthermore, $R_{1\rho}$ is also nonlinearly dependent on the $k/\Delta\omega$ ratio.[6] These nonlinearities are apparent in Figure 5A as catalysis is less pronounced at high phosphate concentrations. Our results indicate that adenosine phosphates have smaller effect on $R_{1\rho}$ in comparison with inorganic phosphates in protein samples (Figures 5A and 5B). This may reflect different acid dissociation constants among the exchangeable protons. Reduction in $R_{1\rho}$ may also have contributions from dipolar relaxation *via* water–water proton exchange processes.[8] This view is supported by the observation that inorganic phosphates abolish the magic angle effect in articular cartilage.[34]

We have previously reported prompt $R_{1\rho}$ decreases in cerebral ischemia. In ischemia, the $R_{1\rho}$ response precedes water diffusion changes by 20 to 30 seconds.[32,35] Conversely, in CSD, diffusion precedes the $R_{1\rho}$ response (Figure 4). These observations are consistent with a reversed order of depolarization and energy consumption events between CSD and ischemia.[18] In CSD, abrupt ion translocation across the neuronal membranes causes water influx, cellular swelling, and decreases in ADC.[18,36] As the Na-K-ATPase activity recovers the ion balance, ATP consumption transiently surpasses mitochondrial ATP production.[15,16] This mismatch between ATP production and consumption may mediate an $R_{1\rho}$ decrease *via* release of inorganic phosphate (Figure 5). In ischemia, prompt O_2 depletion generates a negative BOLD signal, energy substrate exhaustion and acidification cause a decrease in $R_{1\rho}$, which then leads to depolarization and a decrease in ADC. The sequences of these events together with our MRI observations indicate a fundamental difference between the ADC and SL contrast generation mechanisms.[35] Another remarkable difference between CSD and anoxia is the slow recovery of the SL_{6000Hz}(USPIO) response several minutes after the CSD (Figure 4). We propose that this prolonged SL response in comparison with a positive BOLD response is a consequence of intense postCSD metabolic energy deficit, which persists for several minutes after the normalization of cellular ion equilibrium as indicated by the ADC response.[26] This implies that the regulatory mechanisms behind the BOLD signal are not solely driven by neurometabolic energy requirements.

Our SL-fMRI results presented in this manuscript emphasize the importance of thorough investigation for the interpretation of $R_{1\rho}$ origins when multiple relaxation mechanisms and compartments are present. The drawback with the high $B_{1,SL}$ measurement is that it produces high signal absorption rate of energy, which renders it less applicable for human subjects. The functional applications in humans are also limited by functional partial volume changes between parenchyma, CBV, and cerebrospinal fluid,[12,37] and caution should be exercised when interpreting the SL-fMRI signal origin. Intriguingly, our data suggest a new endogenous origin for the SL-fMRI response: $B_{1,SL}$-dependent parenchymal $R_{1\rho}$ decrease may be associated with activity-evoked increase in inorganic phosphate concentration *via* consumption of high-energy phosphates. This links $R_{1\rho}$ to fundamental components of energy metabolism and explains in part our earlier findings in hyperacute stroke.[32] In conclusion, SL-fMRI is sensitive to parenchyma-originated metabolism, has several contributing factors including pH, metabolites, and high-energy phosphates and may be used to map metabolic transitions under controlled experimental settings.

DISCLOSURE/CONFLICT OF INTEREST

The authors declare no conflict of interest.

ACKNOWLEDGMENTS

The authors would like to thank Maarit Pulkkinen for help with preparation of samples. We thank Joanna Huttunen and Juha-Pekka Niskanen for technical support for the data analyses.

REFERENCES

1 Ogawa S, Lee TM, Barrere B. The sensitivity of magnetic resonance image signals of a rat brain to changes in the cerebral venous blood oxygenation. *Magn Reson Med* 1993; **29**: 205–210.
2 Schridde U, Khubchandani M, Motelow JE, Sanganahalli BG, Hyder F, Blumenfeld H. Negative BOLD with large increases in neuronal activity. *Cereb Cortex* 2008; **18**: 1814–1827.
3 Shih YYI, Chen CCV, Shyu BC, Lin ZJ, Chiang YC, Jaw FS *et al.* A new scenario for negative functional magnetic resonance imaging signals: endogenous neurotransmission. *J Neurosci* 2009; **29**: 3036–3044.
4 Le Bihan D, Urayama S, Aso T, Hanakawa T, Fukuyama H. Direct and fast detection of neuronal activation in the human brain with diffusion MRI. *Proc Natl Acad Sci* 2006; **103**: 8263–8268.
5 Kershaw J, Tomiyasu M, Kashikura K, Hirano Y, Nonaka H, Hirano M *et al.* A multi-compartmental SE-BOLD interpretation for stimulus-related signal changes in diffusion-weighted functional MRI. *NMR Biomed* 2009; **22**: 770–778.
6 Trott O, Palmer AG. R1rho relaxation outside of the fast-exchange limit. *J Magn Reson* 2002; **154**: 157–160.
7 Liepinsh E, Otting G. Proton exchange rates from amino acid side chains-implications for image contrast. *Magn Reson Med* 1996; **35**: 30–42.
8 Luz Z, Meiboom S. Rate and mechanism of proton exchange in aqueous solutions of phosphate buffer. *J Am Chem Soc* 1964; **86**: 4764–4766.
9 Mäkelä HI, Gröhn OHJ, Kettunen MI, Kauppinen RA. Proton exchange as a relaxation mechanism for T1 in the rotating frame in native and immobilized protein solutions. *Biochem Biophys Res Commun* 2001; **289**: 813–818.
10 Jin T, Autio J, Obata T, Kim SG. Spin-locking versus chemical exchange saturation transfer MRI for investigating chemical exchange process between water and labile metabolite protons. *Magn Reson Med* 2011; **65**: 1448–1460.
11 Magnotta VA, Heo HY, Dlouhy BJ, Dahdaleh NS, Follmer RL, Thedens DR *et al.* Detecting activity-evoked pH changes in human brain. *Proc Natl Acad Sci* 2012; **109**: 8270–8273.
12 Hulvershorn J, Borthakur A, Bloy L, Gualtieri EE, Reddy R, Leigh JS *et al.* T1rho contrast in functional magnetic resonance imaging. *Magn Reson Med* 2005; **54**: 1155–1162.

13 Jin T, Kim SG. Characterization of non-hemodynamic functional signal measured by spin-lock fMRI. *Neuroimage* 2013; **78**: 385–395.
14 Dalkara T, Nozari A, Moskowitz MA. Migraine aura pathophysiology: the role of blood vessels and microembolisation. *Lancet Neurol* 2010; **9**: 309–317.
15 Mies G, Paschen W. Regional changes of blood flow, glucose, and ATP content determined on brain sections during a single passage of spreading depression in rat brain cortex. *Exp Neurol* 1984; **84**: 249–258.
16 Gault LM, Lin CW, LaManna JC, David Lust W. Changes in energy metabolites, cGMP and intracellular pH during cortical spreading depression. *Brain Res* 1994; **641**: 176–180.
17 Mutch WAC, Hansen AJ. Extracellular pH changes during spreading depression and cerebral ischemia: mechanisms of brain pH regulation. *J Cereb Blood Flow Metab* 1984; **4**: 17–27.
18 Takano T, Tian GF, Peng W, Lou N, Lovatt D, Hansen AJ *et al.* Cortical spreading depression causes and coincides with tissue hypoxia. *Nat Neurosci* 2007; **10**: 754–762.
19 Gröhn OHJ, Michaeli S, Garwood M, Kauppinen RA, Gröhn OHJ. Quantitative T1rho and adiabatic Carr-Purcell T2 magnetic resonance imaging of human occipital lobe at 4 T. *Magn Reson Med* 2005; **54**: 14–19.
20 Autio JAA, Kershaw J, Shibata S, Obata T, Kanno I, Aoki I. High b-value diffusion-weighted fMRI in a rat forepaw electrostimulation model at 7 T. *Neuroimage* 2011.
21 Jin T, Kim SG. Functional changes of apparent diffusion coefficient during visual stimulation investigated by diffusion-weighted gradient-echo fMRI. *Neuroimage* 2008; **41**: 801–812.
22 Does MD, Zhong J, Gore JC. In vivo measurement of ADC change due to intravascular susceptibility variation. *Magn Reson Med* 1999; **41**: 236–240.
23 Kennan RP, Scanley BE, Innis RB, Gore JC. Physiological basis for BOLD MR signal changes due to neuronal stimulation: separation of blood volume and magnetic susceptibility effects. *Magn Reson Med* 1998; **40**: 840–846.
24 Kettunen MI, Gröhn OHJ, Silvennoinen MJ, Penttonen M, Kauppinen RA. Effects of intracellular pH, blood, and tissue oxygen tension on T1rho relaxation in rat brain. *Magn Reson Med* 2002; **48**: 470–477.
25 Cobb JG, Xie J, Gore JC. Contributions of chemical exchange to T1rho dispersion in a tissue model. *Magn ResonMed* 2011; **66**: 1563–1571.
26 de Crespigny A, Röther J, van Bruggen N, Beaulieu C, Moseley ME. Magnetic resonance imaging assessment of cerebral hemodynamics during spreading depression in rats. *J Cereb Blood Flow Metab* 1998; **18**: 1008–1017.
27 Bockhorst KHJ, Smith JM, Smith MI, Bradley DP, Houston GC, Carpenter TA *et al.* A quantitative analysis of cortical spreading depression events in the feline brain characterized with diffusion-weighted MRI. *J Magn Reson Imaging* 2000; **12**: 722–733.
28 Wagner IV SR, Lanier WL. Metabolism of glucose, glycogen, and high-energy phosphates during complete cerebral ischemia: a comparison of normoglycemic, chronically hyperglycemic diabetic, and acutely hyperglycemic nondiabetic rats. *Anesthesiology* 1994; **81**: 1516–1526.
29 Fabricius M, Jensen LH, Lauritzen M. Microdialysis of interstitial amino acids during spreading depression and anoxic depolarization in rat neocortex. *Brain Res* 1993; **612**: 61–69.
30 Hashemi P, Bhatia R, Nakamura H, Dreier JP, Graf R, Strong AJ *et al.* Persisting depletion of brain glucose following cortical spreading depression, despite apparent hyperaemia: evidence for risk of an adverse effect of Leao's spreading depression. *J Cereb Blood Flow Metab* 2008; **29**: 166–175.
31 Kogan F, Haris M, Singh A, Cai K, Debrosse C, Nanga RPR *et al.* Method for high-resolution imaging of creatine in vivo using chemical exchange saturation transfer. *Magn Reson Med* 2013; **71**: 164–172.
32 Gröhn OHJ, Kettunen MI, Mäkelä HI, Penttonen M, Pitkänen A, Lukkarinen JA *et al.* Early detection of irreversible cerebral ischemia in the rat using dispersion of the magnetic resonance imaging relaxation time, T1rho. *J Cereb Blood Flow Metab* 2000; **20**: 1457–1466.
33 Gröhn OH, Lukkarinen JA, Silvennoinen MJ, Pitkänen A, van Zijl P, Kauppinen RA. Quantitative magnetic resonance imaging assessment of cerebral ischemia in rat using on-resonance T1 in the rotating frame. *Magn Reson Med* 1999; **42**: 268–276.
34 Zheng S, Xia Y. Effect of phosphate electrolyte buffer on the dynamics of water in tendon and cartilage. *NMR Biomed* 2009; **22**: 158–164.
35 Kettunen MI, Gröhn OHJ, Penttonen M, Kauppinen RA. Cerebral T1rho relaxation time increases immediately upon global ischemia in the rat independently of blood glucose and anoxic depolarization. *Magn Reson Med* 2001; **46**: 565–572.
36 Zhou N, Gordon GRJ, Feighan D, MacVicar BA. Transient swelling, acidification, and mitochondrial depolarization occurs in neurons but not astrocytes during spreading depression. *Cereb Cortex* 2010; **20**: 2614–2624.
37 Piechnik SK, Evans J, Bary LH, Wise RG, Jezzard P. Functional changes in CSF volume estimated using measurement of water T2 relaxation. *Magn Reson Med* 2009; **61**: 579–586.

Supplementary Information accompanies the paper on the Journal of Cerebral Blood Flow & Metabolism website (http://www.nature.com/jcbfm)